ORIGINAL RESEARCH

Finite element method simulation of the hot extrusion of a powder metallurgy stainless steel grade

D. Sornin · A. Karch · D. Nunes

Abstract Oxides Dispersed strengthened (ODS) stainless steels are foreseen for fuel cladding tubes in the coming generation of fission nuclear reactors. In spite of a ferritic matrix those steels present a convenient creep behavior thanks to very fine oxides dispersion. Those grades are currently obtained by Powder Metallurgy (PM). After mechanical alloying with the oxide, the powder is commonly consolidated by Hot Isostatic Pressing (HIP) or Hot Extrusion (HE). The control of microstructure after extrusion is a key issue for this grade regarding service conditions. On CEA facilities, new ferritic ODS stainless steels are produced by HE. In order to explain the microstructure observed at various places on an interrupted extrusion samples the thermo-mechanical history applied to the material must be determined. In this paper we use the Finite Element Method to simulate the co-extrusion of a PM grade in a soft steel can. The PM steel grade behavior law is determined on a fully dense material by hot torsion tests, taking into account temperature and strain-rate sensitivity. Thus strain and thermal history are computed for material points lying on various flow lines during extrusion.

Keywords Hot extrusion · Powder metallurgy · Finite element method · Numerical modeling · Oxides dispersed strengthened steel

D. Sornin · A. Karch · D. Nunes
CEA, DEN, Service de Recherches Métallurgiques Appliquées, 91191 Gif-Sur-Yvette, France

D. Sornin (✉)
DEN/DANS/DMN/SRMA, PC52 bât460, CEA Saclay, 91191 Gif-Sur-Yvette, France
e-mail: denis.sornin@cea.fr

Introduction

Ferritic Oxides Dispersed Strengthened stainless steels are promising candidates for many nuclear applications due to their behavior under strong irradiation [1]. Such materials are commonly foreseen for the fuel cladding tube of Sodium Fast Reactors [2]. They show good mechanical behavior at high temperature (exceeding 600 °C) [3] under severe irradiation (more than 150 Displacement Per Atoms) [4]. Regarding corrosion aspects, high chromium stainless steels are preferred. The choice of a ferritic or ferritic/martensitic microstructure reduces drastically void swelling under irradiation [5]. The creep behavior is enhanced by a very fine dispersion of stable Y-Ti-O nano-clusters. This fine dispersion acts on both the dislocation mobility [6] and the grain size (100–500 nm) [7]. For better mechanical properties, the manufacturing process should produce a homogenous distribution of nano-sized oxides in a fine grain matrix. To reach this goal, ODS steel are generally produced by powder metallurgy [8]. Oxides are dissolved in the metallic powder by mechanical alloying at ambient temperature. To produce cladding tubes, the ODS material must be consolidated and shaped as long and seamless rough tubes. Hot Extrusion (HE) of hollow section is commonly used in such cases. After milling, the loose powder is directly (without previous consolidation) processed by HE in a sealed can on the CEA facilities. After hot extrusion the material presents a heterogeneous grain size from 50 nm to a few microns [9]. This microstructure presents strong crystallographic and morphological texture [10], and mechanical anisotropy [3] to the detriment of the hoop direction. With a view towards to reduce this anisotropy, studies are driven to better understand the role of hot forming. Texture and microstructure in the extruded tube are important features for applications as they modify the material response during subsequent heat treatments and/or applications. To better understand metallurgical evolution during hot forming the HE

process must be studied. Instrumentation of the experiment is excessively complex and expensive. That is the reason why flow lines and the associated thermo-mechanical loading are to be determined by numerical modeling. Whereas several numerical models of porous media plasticity have been proposed for HIP modeling [11], few proposals address the modeling of Hot Extrusion of powders. The present paper focuses on the Finite Element Method (FEM) modeling of the consolidation by HE of loose powder sealed in a can. The thermo-mechanical history will be determined for specific material points at different time during flowing throughout the die. Those results will help in two ways to a better understanding of hot extrusion. First the thermo-mechanical conditions occurring during HE will be determined. Secondly, the deduced loading could be used as an input for metallurgical modeling in order to determine the grains shape, grain size and crystallographic texture evolution.

The experimental hot extrusion process

Material manufacturing

The ODS steel was produced by powder metallurgy techniques. The initial stainless steel powder was gas atomized under Argon and presents spherical shape with a characteristic mean size about 50 μm. This powder was mechanically alloyed together with 0.3 wt% Y_2O_3 on industrial attritors by PLANSEE under hydrogen atmosphere. After mechanical alloying the powder presents a uniform composition of Fe-14Cr-1 W-0.3Ti-0.25Y_2O_3 (wt%) and mean particle size was about 80 μm. For consolidation by HE, a soft steel can was prepared by charging with the mechanically alloyed powder. The billet was then capped and arc welded in air. It was subsequently vacuumed at 4 10^{-7} mbar and 400 °C during 2 h. Then the billet was placed in a furnace and heated in air at 1,100 °C for 1 h. The heating rate is about 40 °C.min^{-1}. This means that the dwell time at 1,100 °C is about 30 min. This heating leads to precipitation of nano-oxides [12]. The preheated billet was then placed into a press and hot extruded to obtain tubes or bars.

The hot extrusion process

The extrusion is performed on a vertical 575 t press. The hot billet is placed in a Ø75 mm container. Under the container a 90° conical die is placed with a circular hole of 21 mm. A copper seal is placed on the ram to avoid back flowing of the material during processing. The container and the die are heated at 380 °C. The lubrication is performed by slices of graphite placed on each extremity of the ingot before extrusion. The extrusion itself was performed within 10 s and the extruded rod is air cooled. The can geometry is about 240 mm long and 72 mm in diameter. Before introduction into furnace, the loose powder fills a 180*Ø60 mm

cylinder, inside the can, with a relative density of about 58 %. This corresponds approximately to 2.5 Kg of steel powder. A small tube in the head is used to vacuum the powder during the preparation of the billet. During the first seconds of the process, the powder is compacted and, simultaneously, the clearance between the billet and the container is filled. At this point the extrusion force strongly increases to reach 340 t. A recent study shows that the PM grade reaches a fully dense state before passing throughout the die [13]. After this stage of compaction, the can walls are thicken and the ODS steel ingot presents a Ø56.5 mm diameter. In a second step the PM grade is co-extruded with the can just like standard materials. The extrusion ratio is commonly chosen from 10 to 20 to avoid an excessive extrusion force. This process drives to the production of Ø21 mm rod of a few meters long with an outer skin of soft steel. The interface between the ODS steel and the soft steel is tight, therefore the outer skin must be removed by machining or chemical processes before cold forming operations.

The reference sample

Specific samples based on interrupted extrusion are elaborated. This allows to access to the working region. The ram displacement is stopped after 170 mm and preserve material in the upstream of the die. Figure 1a presents a scheme of the interrupted HE cross section where the ODS steel ingot is enclosed into the can.

The obtained billet is extracted from the container and cut along the extrusion axis by Electric Discharge Machining (EDM) wire cutting (Fig. 1b), enabling microstructural studies along flow lines.

Hot torsion test

Torsion samples

In order to drive FEM simulations the constitutive law for the PM grade must be determined at high temperature under high strain rates. Due to a very strong textural and morphological anisotropy after HE the ODS steel grade samples cannot be extracted from extruded rods. Torsion tests are preferred to the standard tensile test to avoid early damaging and to achieve higher strain rates. Consequently, we decide to drive hot torsion tests on the fully consolidated material placed in the un-extruded region (see Fig. 1a). This material is shown to be fully dense and isotropic with an heterogeneous grain size microstructure from 100 nm to a few microns [13]. By EDM wire cutting, 10 mm cylindrical rods are extracted from the ingot and machined as torsion test samples. The obtained geometry is presented at Fig. 2.

Those samples are cylinders with Ø4.5 mm in diameter and 11.6 mm long gauge section. The small amount of material

Fig. 1 Geometry of the HE apparatus (**a**) cross section scheme, (**b**) the reference sample
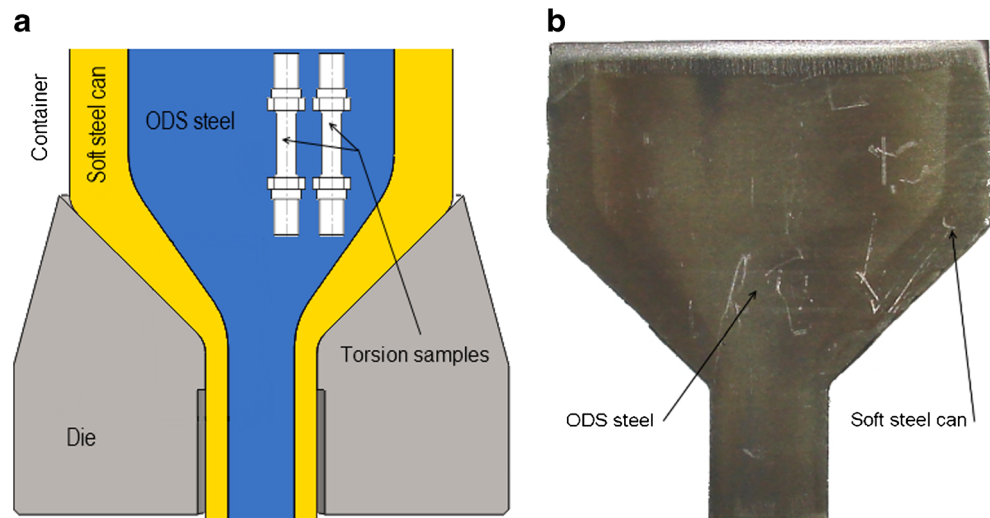
available coupled to a very fine microstructure drive us to choose this small geometry by comparison with standard samples. Screwed mandrels presented at Fig. 2b enable adaptation to the torsion machine.

Experimental conditions

The test conditions prospect three levels of strain rate (0.05, 0.5 and 5 s−1) and three levels of temperature (1,000, 1,100, 1, 200 °C). Those temperatures and strain rates tend to simulate the conditions encountered during the hot extrusion. The torsion couple versus angle position is recorded and these data are treated by the Fields & Backofen method [14] to obtain the stress–strain curves. The samples are heated to the torsion temperature in a radiating oven enabling heating rate of 5 K.s−1. A center hole placed in the fixed mandrel extremity enables to introduce a thermocouple just near the deformation zone. This thermocouple will capture the temperature during the heating and the torsion test itself. The thermal control of the oven is performed with this probe information.

Tests are driven at constant current in furnace trying to determine the Joule effect induced by plasticity. Therefore it is possible to know the increase in the temperature measured by the central thermocouple. In most cases the temperature increment is less than 20 °C, so the assumption of isothermal tests could be considered for the stress–strain curve determination (Fields & Backofen method). Unfortunately it is impossible to determine correctly the percentage of plastic work dissipated in heating during the hot deformation.

Stress–strain results

Figure 3 presents the equivalent Von-Mises stress as a function of cumulated plastic strain for 3 levels of plastic strain rate from 0.05 s^{-1} to 5 s^{-1}.

As suspected, rising strain rate increases the flowing stress whatever the temperature. The effect of temperature increase is a global softening. Compared to a similar ferritic stainless steel [15], this ODS steel grade exhibits a higher flow stress but a lower ductility. These two aspects are probably strongly linked to the very fine dispersion of nano-precipitate that reinforces the matrix.

Numerical modeling of the hot extrusion of loose powder

Large strain FE formulation

The formulation chosen in this study relies on the multiplicative decomposition of the total deformation gradient $\underline{F}$ (underscore indicate tonsorial quantities) into an inelastic component $\underline{F}^p$ and an elastic component $\underline{F}^e$.

$$\underline{F} = \underline{F}^e \cdot \underline{F}^p \tag{1}$$

As discussed above the PM grade is fully dense before extrusion throughout the die. Consequently the assumption of incompressible plasticity is retained for both the can and the core. It follows that $\det \underline{F} = \det \underline{F}^e$ assuming $\det \underline{F}^p = 1$.
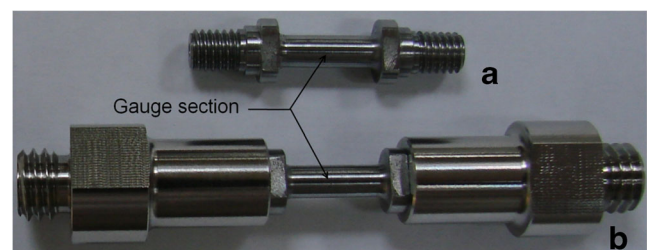

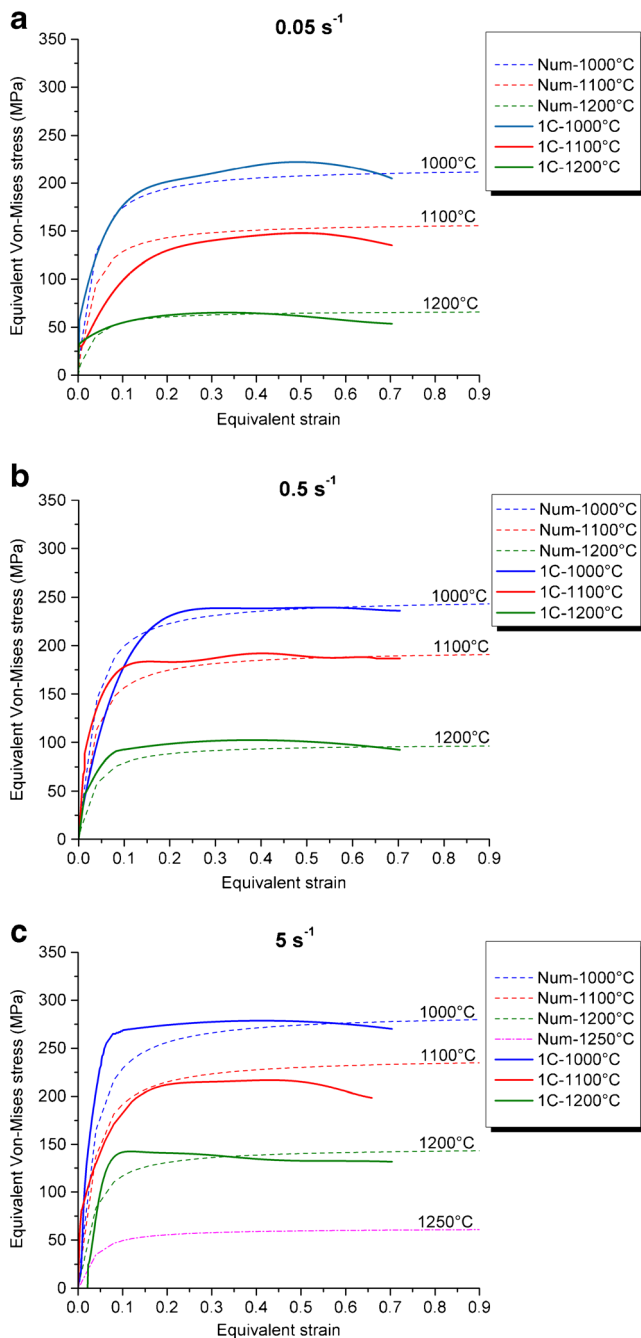**Fig. 2** Geometry of the torsion samples, (**a**) without mandrels (**b**) with the mandrels apparatus

Fig. 3 Stress–strain curves for three levels of temperature, (**a**) at 0.05 s^{-1}, (**b**) at 0.5 s^{-1}, (**c**) at 5 s^{-1}

Applying the standard finite element Galerkin discretization process with the approximation of displacement as $u(\xi) = \sum_k N_k(\xi) u_k$ it derives from the equilibrium equation

$$R = \int_\Omega \left(B^T \underline{F} \right) : \underline{S} - \int_\Omega N^T \{f_v\} = 0 \qquad (2)$$

Where the residual R is a function of the shape function N of the element, B is defined by the shape function derivatives,

S the second Piola-Kirchhoff stress and $\{f_v\}$ the vector of the volumetric forces. In order to solve the problem by a Newton–Raphson scheme the variation of the residual with respect to displacement is determined as

$$dR = \int_\Omega \left(B^T \underline{F} \right) : d\underline{S} + \int_\Omega \left(B^T d\underline{F} \right) : \underline{S} = K^{mat} du_k + K^{geom} du_k$$

$$(3)$$

The first and second terms correspond to the material and the geometrical contribution to the tangent stiffness matrix respectively. The determination of the contribution of inelastic part to the material tangent stiffness matrix is described below.

Simulation set up

This simulation is based on the extrusion process geometry presented in "The reference sample" section. Regarding the geometries of the ingot and the tools the assumption of axi-symmetry is retained to avoid an excessive computational cost. Simulation are driven using the industrial FEM code MSC-MARC2012. The initial geometry of the ingot (Fig. 4a) is chosen to fit with the dimensions observed on interrupted extrusion samples; it means, a Ø62 mm core in a Ø75 mm can. All the tools are assumed rigid and isothermal bodies. The interface between the can and the core is considered as a glue type; it means that normal and tangential relative displacements are blocked.

Boundary conditions

The can is considered in contact with the container as an initial condition. The temperature is fixed at 380 °C for the die and the container and 50 °C for the ram. Contacts between the can and the rigid tools are assumed sliding with friction following a Coulomb-Tresca like model. Friction coefficient is chosen at 0.05 for the lubricated contact with a maximum shear stress of 250 MPa. In all cases the contact algorithm is penalty. The ram velocity is assumed constant and fixed at 25 mm.s^{-1}. The die and the container are fixed. A displacement condition is assumed for the nodes lying on the revolution axis to warranty the axi-symmetry. The interface between the two materials is assumed thermally perfect; it means that the same temperature is imposed on both materials at the interface. Thermal interactions at tools/can interfaces are pure conduction with a conduction parameter equal to 0.5 W.K^{-1}.mm^{-1}. It takes into account the effect of lubricant an oxidation of the billet skin. A general radiation in air condition is applied on the external surfaces of the billet except the one in contact with the ram to model the air cooling of the extruded product. This last condition is shown to have a small impact on the early stage of extrusion. At initial condition, the temperature at all the nodes

Fig. 4 Meshing definition of, (a) the initial ingot, (b) the die region refinement during extrusion with LC, LM flow lines positions
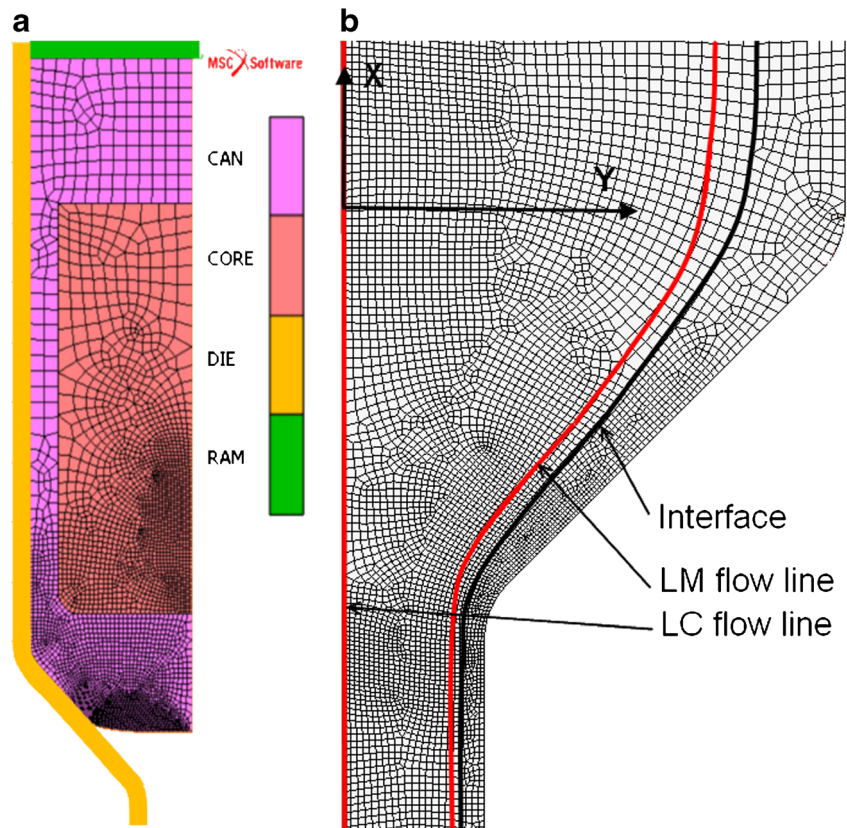
of the ingot is prescribed at 1,100 °C. The heating generated by friction is taken into account with 15 % of the friction energy dissipated by Joule effect in the can. The Taylor-Quinney parameter is assumed constant at β=90 % and similar for the core and the can materials during the whole process.

Meshing

Regarding precision and computational cost we choose a bilinear exactly integrated element for both the can and the core. Those bodies are remeshed during processing following a criterion based on the element distortion and the plastic strain level. More than 250 remeshing are needed to avoid element distortion and penetration at contact edges. The mesh size is controlled via remeshing boxes placed on the flowing region with four levels of refinement. The final meshing is described at Fig. 4b. A general mesh size of 3 and 4 mm are chosen for the can and the core respectively, with a minimal mesh size at 0.2 mm.

Identification of the constitutive laws

From the results presented in Fig. 3a constitutive law can be identified. A Prandtl-Reuss model is considered with the following expression of the yield locus

$$f\left(\underline{\sigma}, T\right) = \left\|\underline{\sigma}\right\| - \sigma_0 \tag{4}$$

Where $\left\|\underline{\sigma}\right\|$ the equivalent Von-Mises is stress and σ_0 defined by

$$\sigma_0 = \left(\sigma_y + Ae^{-\left(\frac{n1}{\overline{\varepsilon}}\right)} \cdot \dot{\overline{\varepsilon}}^{\frac{n2}{[T_s-T]}}\right) e^{\frac{-n3}{[T_s-T]}} \tag{5}$$

where σ_y is the yield stress, $\overline{\varepsilon}$ is the equivalent plastic strain, $\dot{\overline{\varepsilon}}$ is the equivalent plastic strain rate, T the temperature (in °C) and $A, n1, n2, n3, T_S$ are constant parameters. Accordingly to *Praud and al* [16], the young modulus E and Poisson ratio v are chosen at 120 GPa and 0.3 respectively. Determination of the constitutive law parameter is performed iteratively to obtain a convenient fit between the computed and experimental curves. The superposition of the model (dot lines) and the experimental curve is presented for each condition at Fig. 3. The Table 1 presents the experimental flow stress (column 3) and the prediction of the model of Eq. 5 (column 4).

Finally, the percentage difference between the computed flow stress and the experimental one is presented in the last column. The identification is driven to reduce the maximum deviation under 10 %. Following the same strategy the soft steel can behavior is identified on 6 torsion tests driven at

Table 1 Comparison of experimental and model flow stress

N°	Conditions	Flow stress (MPa)		Difference
		Experimental	Model	(%)
1	1,000 °C/0.05 s−1	220	213	3.6
2	1,100 °C/0.05 s−1	148	156	5.8
3	1,200 °C/0.05 s−1	65	66	1.7
4	1,000 °C/0.5 s−1	237	244	2.9
5	1,100 °C/0.5 s−1	187	192	2.4
6	1,200 °C/0.5 s−1	105	97	7.8
7	1,000 °C/5 s−1	272	281	3.2
8	1,100 °C/5 s−1	216	236	9.3
9	1,200 °C/5 s−1	132	144	8.8

0.15 s^{-1}, 1.5 s^{-1} and 15 s^{-1} at two levels of temperature 1,000 °C and 1,200 °C. These results are consistent with bibliographic data [17]. The model parameters, expressed in MPa, are presented for both the PM steel core and the soft steel can in Table 2.

Using the constitutive equation (Eq. 5) a user subroutine WKSLP is coded in Fortran 77 and integrated in the MSC-MARC finite Element code. Likewise, the stress triaxiality is computed as the ratio of the first and second invariant of the stress tensor.

- Tangent stiffness

The MSC-MARC code uses an implicit integration scheme. Therefore a tangent stiffness must be output from the behavior routine WKSPL. This routine deals with the computation of hardening in the elasto-plastic scheme. The elastic contribution to the tangent stiffness is automatically computed by the code from furnished elastic constants. Therefore to compute the continuum tangent modulus the user needs to define the slope of the equivalent stress vs; equivalent plastic strain and plastic strain rate. For the model defined at Eqs. 4 and 5, the hardening contribution to the tangent modulus is the sum of two terms detailed at Eqs. 7 and 8. Those terms correspond to the variation of the equivalent stress regarding equivalent plastic strain and strain rate,

$$\frac{d\|\underline{\sigma}\|}{d\overline{\varepsilon}^p} = \frac{\partial\|\underline{\sigma}\|}{\partial\overline{\varepsilon}^p} + \frac{\partial\|\underline{\sigma}\|}{\partial\dot{\overline{\varepsilon}}^p}\frac{d\dot{\overline{\varepsilon}}^p}{d\overline{\varepsilon}^p} = \frac{\partial\|\underline{\sigma}\|}{\partial\overline{\varepsilon}^p} + \frac{\partial\|\underline{\sigma}\|}{\partial\dot{\overline{\varepsilon}}^p}\frac{1}{\Delta t} \quad (6)$$

with

$$\frac{\partial\|\underline{\sigma}\|}{\partial\overline{\varepsilon}^p} = e^{\frac{-n3}{[TS-T]}}\left(Ae^{-\left(\frac{n1}{\overline{\varepsilon}}\right)}\cdot\dot{\overline{\varepsilon}}^p\frac{n2}{[T_S-T]}\right)\frac{n1}{\overline{\varepsilon}^2} \quad (7)$$

$$\frac{\partial\|\underline{\sigma}\|}{\partial\dot{\overline{\varepsilon}}^p} = e^{\frac{-n3}{[TS-T]}}\left(Ae^{-\left(\frac{n1}{\overline{\varepsilon}}\right)}\cdot\dot{\overline{\varepsilon}}^p\frac{n2}{[T_S-T]}\right)\frac{n2}{[T_S-T]}\frac{1}{\dot{\overline{\varepsilon}}} \quad (8)$$

where σ is the stress tensor, Δt the time increment. $\|\underline{\sigma}\|$ and $\overline{\varepsilon}^p$ represent equivalent stress and equivalent plastic strain respectively. Those terms are coded and return as well as the updated stress for each integration point. The tangent modulus associated to temperature $\frac{\partial\sigma}{\partial T}$ is assumed insignificant and neglected in the computation.

Results

Strain and geometry

Figure 5a presents the filled contours of cumulated plastic strain.

The results are presented for a permanent flow condition at $t=2$ s after the first movement of the RAM. Logically, the plastic strain is strongly increasing with the reduction of section. The maximum of plastic strain is noticed for the inner face of the canning. Figure 6 presents the values of cumulated plastic strain and equivalent of plastic strain along the radius of the extruded bar.

At the center of the bar (position =0) the two curves are superimposed. On the core/can interface ($r=8.7$ mm) a significant difference is noticed due to the shearing generated by the die angles. The sum of positive and negative shearing during extrusion is approximately zero. As a consequence, the equivalent of plastic strain is relatively constant along the radius path. Because of the glue condition of contact between core and can, a strong discontinuity is noticed at the interface. Both cumulated and equivalent of plastic strain are higher in the can than in the core. From a mechanical point of view the canning plays the role of protection of the core and enables a constant level of equivalent plastic strain in the product. The outer diameter of the ODS core is computed at Ø 17.4 mm in a Ø 21 mm rod. This fits fairly well with the experimental values measured at Ø 17.33 mm.

Temperature

Figure 5b plots filled contours of nodal temperature. Temperature is increasing from 1,100°c in the ingot core (the initial condition) to 1,250°c in the extruded PM stainless steel bar. This increase is due to the Joule effect. Considering the high level of flow stress, the Joule effect drives to more than 150 °C of warming. This phenomenon, inducing the thermal softening of the PM ODS grad, is essential to enable hot extrusion in an acceptable level of extrusion force. In Fig. 7, ram force curves are plotted for various values of the Taylor-Quinney coefficient β from 55 % to 95 %.

Table 2 Constitutive law parameters for both the PM grade and the soft steel

	σ_y	A	n1	n2	n3	TS	E	ν
ODS PM steel	40	375	0.025	21	145	1,310	120,000	0.3
C22 steel	85	180	0.075	130	600	1,480	120,000	0.3

Due to the thermal softening, the higher is the coefficient beta, the less is the force. We note that the extrusion force is slightly impacted by the Taylor-Quinney coefficient.

Stress and forces

Figure 8a presents the filled contours of equivalent Von-Mises stress and pressure.

Obviously, during the process the pressure is highly negative and reaches approximately 550 MPa. Positive pressures are only noticed after the output of the die. Surprisingly, a significant difference is noticed between the can and the core regarding the position of the maximum von-Mises stress. For the core, the higher values are noticed in the conical region (between the two angles of the die) and tend to be reduced by the thermal softening in the die output region. For the can, unlike the core, the strain rate effect increases the Von-Mises stress in the die output region. This phenomenon can be explained both by the difference of strain rate sensitivity between the two materials and the thermal cooling of the can induced by the tools. As for the plastic strain, significant gradients of Von-Mises stress are noticed at the can/core interface.

Figure 7 presents the extrusion force applied to the ram from numerical computation (dash lines) and experimental measurements (plain lines). Experimental curves, noted "Exp", show extrusion force maximum at 390 t whereas numerical simulation exhibits maximums at about 240 t. The 150 t difference is probably manly due to the role of the apparatus used to avoid leakage of lubricant and not taken into account in the numerical simulation. The simulation curves, as well as the experimental ones, present the same shape. In the first step (region 1 in Fig. 7), an extremum in extrusion force is noticed associated to the can head flowing throughout the die. Then force increases until the flowing of the PM ODS grade throughout the die. After this second top the extrusion force remains approximately stable. This last region is assumed to correspond to the established extrusion conditions. This is the reason why computations are driven on the 2 first seconds of the process. The difference noticed between simulation and experiment before the region 1 is due to the compressive behavior of the powder during the early stage of extrusion. From time −1 to 0 s, the powder is consolidated in the experimental conditions whereas for numerical simulation the assumption of incompressible plasticity is retained. This difference tends to vanish in region 1 when powder compaction is achieved. On Fig. 7a numerical curve (Force-Num-0.25) is obtained by changing the friction Coulomb coefficient from 0.05 to 0.25. The extrusion force is logically increased and the maximum of force is achieved earlier compared to the other curves.

Fig. 5 Filled contours, (**a**) cumulated plastic strain, (**b**) temperature (°C)
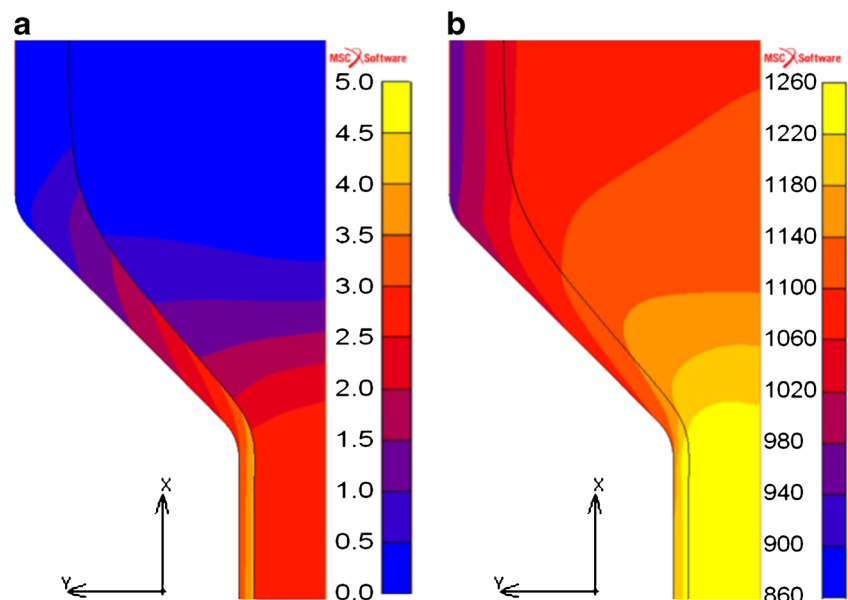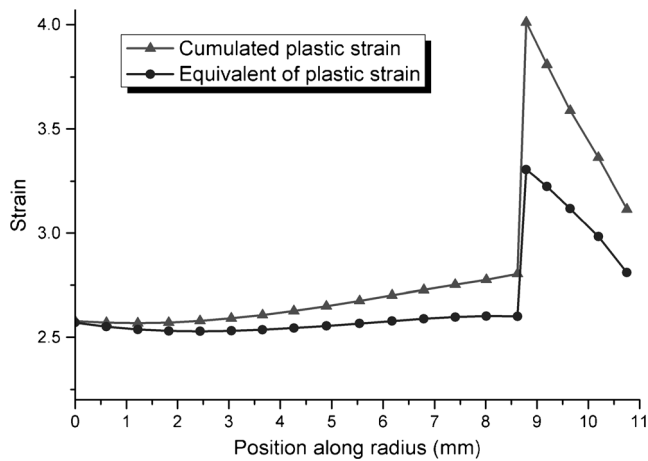
Fig. 6 Plastic strain along a radial path

Strain rate

Figure 9a presents filled contours of equivalent strain rate.

Regarding only the core the maximum of strain rate is obtained in a narrow band and reaches 25 s^{-1} approximately. This value is too high to be reached by standard mechanical tests machines and too low to be prospected by high speed systems like Hopkinson bars [18]. Therefore the strain rate sensitivity of the material during HE must be extrapolated by the behavior law from lower strain rate levels. Stress triaxiality is plotted in Fig. 9b. According to Bao et al. [19], we assume that when stress triaxiality is lower than −1/3 no macroscopic damage occurs. In Fig. 9 there is no superimposition of regions plastically active (strain rate >0) and submitted to damage occurrence (triaxiality > −1/3). This explains the capacity of HE to perform fully dense and undamaged

consolidation of highly damaging material even under very strong plastic strain conditions.

Histories along flow lines

In order to track metallurgical evolution during hot forming two flow lines are retained. The first one (LC) is centered on the revolution axis of the billet. The second one (LM) is placed at 90 % of the external radius of the core. This choice allows us to determine heterogeneity of loading inside the extruded product. Those two lines are extreme conditions of the process far enough from the interface with the soft steel can. In Fig. 10, the cumulated plastic strain is plotted as a function of the position along the extrusion axis.

The origin of the abscissa is placed at the upper corner of the die (see Fig. 4b). Basically, before this point, plastic strain evolves slowly because the section of the product is not reduced. Then the cumulated plastic strain increase until the die output and remains constant for positions far from −32 mm. As discussed in "Strain and geometry" section the cumulated plastic strain is higher for the external flow line (LM). Figure 11 presents, for the two flow lines LC and LM, the equivalent plastic strain rate.

The maximum of strain rate is noticed for the LM flow line just before the die output. The difference observed between the two flow lines can be explained by the shearing strain. The major part of the strain is applied in a very short time about 0.5 s. For temperature versus position in Fig. 12, the tendencies are different for the two flow lines.

For the central flow line (LC) the Joule effect generates a significant increase of the temperature from 1,100 °C, at initial conditions, to 1,225 °C at the die output. For the LM flow line,

Fig. 7 Extrusion force, experimental versus numerical curves
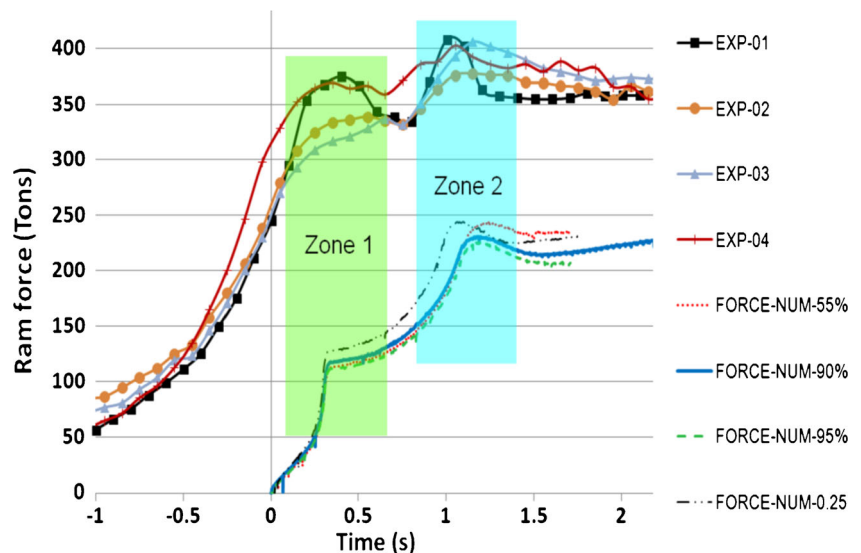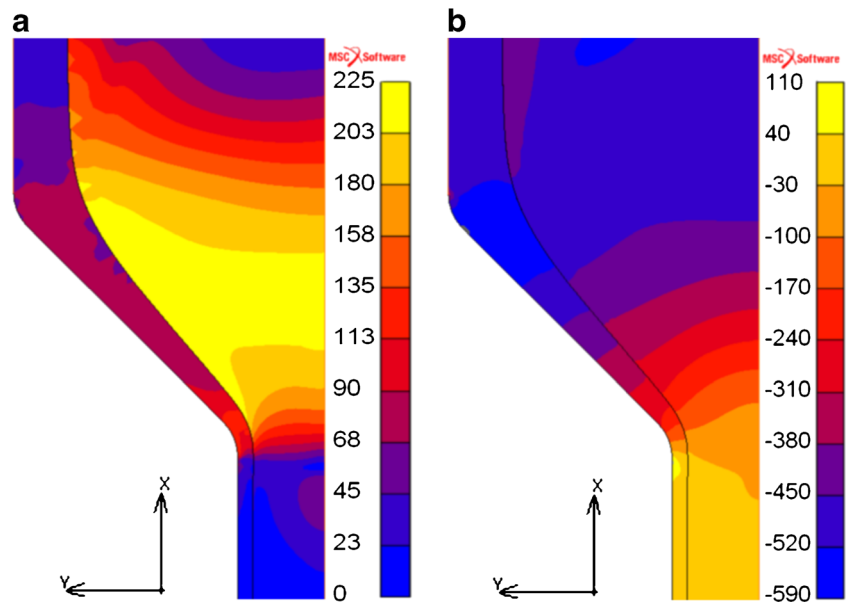
Fig. 8 Filled contours, (**a**) Von-Mises stress (MPa), (**b**) pressure (MPa)

the thermal boundary condition with the container generates a cooling (about 10 °C) before the plastic flow. After extrusion ($t > 1.9$ s) a significant cooling of 9 °C is observed. The reason of this phenomenon is the lower temperature of the soft steel can after extrusion. Indeed the lower flow stress in the soft steel can induces a lower Joule effect and a lower temperature after extrusion. In Fig. 13, along flow lines, the first and second invariants of stress are displayed as function of time.

Recording starts with the first movement of the ram and the die output occurs at time $t = 1.9$ s. For the two flow lines (extension LC and LM) the deviatoric and hydrostatic stress

level are quite similar. The pressure reaches high values of about 5,500 bars during the established flowing. The deviatoric stress is measured at about 200 MPa and seem to remain rather constant during flowing throughout the die (from $t = 1$ to 1.9 s).

Conclusion and perspectives

In this study, an ODS steel was produced by HE of a milled powder. After a description of the different step of the

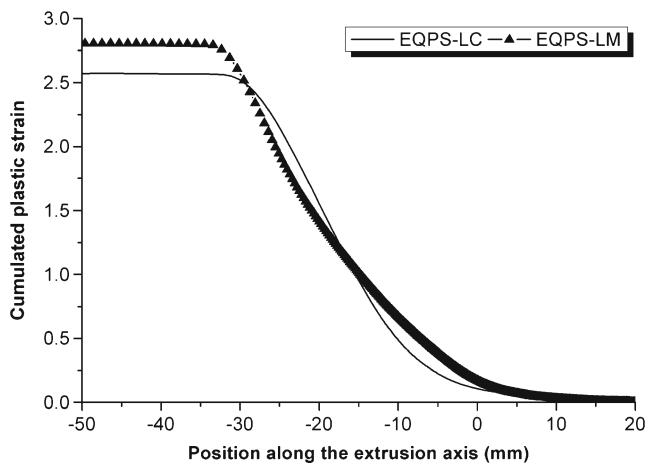**Fig. 9** Filled contours of, (**a**) equivalent strain rate (s−1), (**b**) stress triaxiality
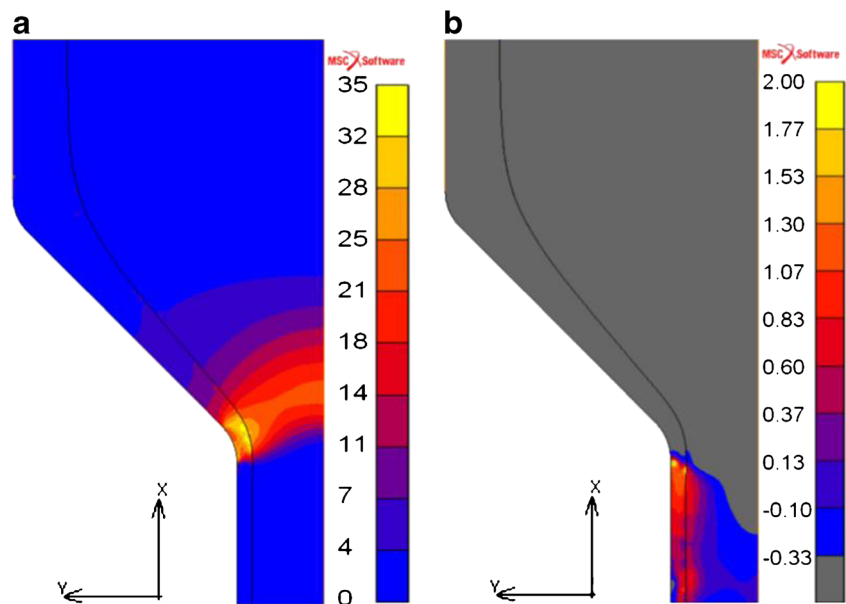
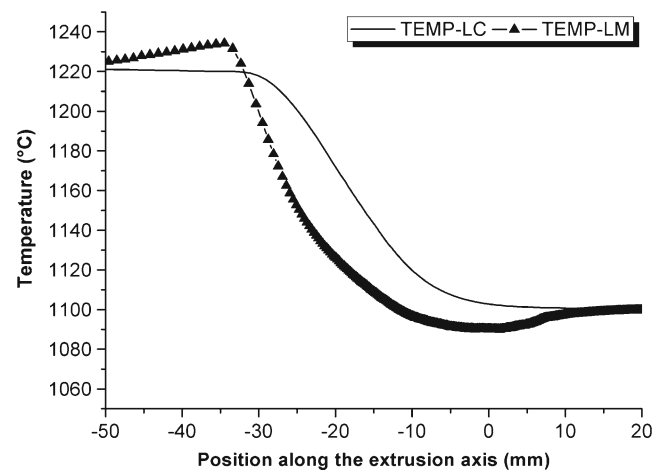Fig. 10 Cumulated plastic strain along flow lines

Fig. 12 Temperature along flow lines

experimental process a numerical modeling is proposed. Using FEM, the co-extrusion of the ODS grade sealed in a soft steel can is performed. The main results can be summarized as follow:

- During the Hot Extrusion, the initially loose powder is fully consolidated before passing throughout the die. This allows running the simulation considering incompressible plasticity for the both materials.
- In order to achieve torsion tests, fully consolidated samples are extracted from an interrupted extrusion test. These samples are representative of the material behavior before extrusion throughout the die. Constitutive laws are obtained for the PM steel core and the soft steel can at high temperature and strain rate. Achieved ductility is too low to determine the behavior for high plastic strain ($\varepsilon_p > 0.8$).
- At any time in the process the stress triaxiality is lower than −1/3 when plastic strain occurs. This means that no macroscopic damage can take place during the extrusion

process, even under strong straining. This explains why a fully dense and undamaged material is obtained by HE even at the canning interface.
- During the processing of such ODS steel grades the Joule effect, estimated at 150 °C, induces a significant thermal softening. Elaboration conditions during HE are numerically estimated about 1,225 °C and 25 s^{-1}.
- The use of a thick canning enable to obtain a rather constant level of strain and strain rate in the extruded section
- Friction coefficients as well as Joule effect are shown to impact slightly the computed extrusion force.

The thermo mechanical loadings of material points lying on two flow lines are determined. Those histories can now be used as inputs for modeling metallurgical evolutions. Microstructural and mechanical characterizations of samples extracted from the interrupted extrusion test are under progress.
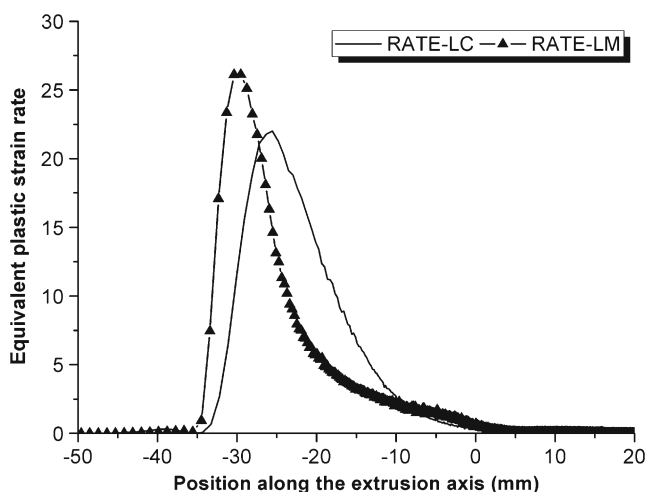

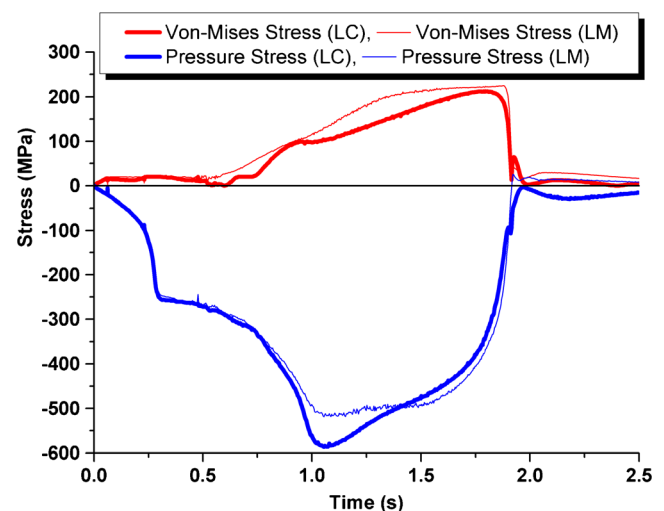Fig. 11 Equivalent plastic strain rate along flow lines

Fig. 13 Stress as function of time for the two flow lines

References

1. de Carlan Y, Bechade J-L et al (2009) CEA developments of new ferritic ODS alloys for nuclear applications. J Nucl Mater 386–388: 430–432
2. Ukai S, Hatakeyama K et al (2002) Consolidation process study of 9Cr-ODS martensitic steels. J Nucl Mater I. 307-311:758–762
3. Steckmeyer A, Praud M, Fournier B, Malaplate J, Garnier J, Béchade JL, Tournié I, Tancray A, Bougault A, Bonnaillie P (2010) Tensile properties and deformation mechanisms of a 14Cr ODS ferritic steel. J Nucl Mater 405(2):95–100
4. Hoelzer DT, Bentley J, Sokolov MA, Miller MK, Odette GR, Alinger MJ (2007) Influence of particle dispersions on the high-temperature strength of ferritic alloys. J Nucl Mater 367-370(Part 1):166–172
5. Alamo A, Lambard V, Averty X, Mathon MH (2004) Assessment of ODS-14%Cr ferritic alloy for high temperature applications. J Nucl Mater 329-333(Part 1):333–337
6. Auger MA, Leguey T, Muñoz A, Monge MA (2011) Microstructure and mechanical properties of ultrafine-grained Fe-14Cr and ODS Fe-14Cr model alloys. J Nucl Mater 417:213–216
7. Dou P, Kimura A, Okuda T, Inoue M (2011) Effect of extrusion temperature on the Nano-mesoscopic structure and mechanical properties of an Al-alloyed High-Cr ODS ferritic steel. J Nucl Mater 417(1–3):166–170
8. Miller MK, Russell KF, Hoelzer DT (2006) Characterisation of precipitates in MA/ODS ferritic alloys. J Nucl Mater 351:261–268
9. Olier P, Malaplate J, Mathon MH, Nunes D, Hamon D, Toualbi L, de Carlan Y, Chaffron L (2012) Chemical and microstructural evolution on ODS Fe-14CrWTi steel during manufacturing stages. J Nucl Mater 428(1-3):40–46. doi:10.1016/j.jnucmat.2011.10.042
10. Praud M, Mopiou F, Malaplate J (2010) Plasticity of nano-strengthened steels. Nucl Mater Conf NuMAt 2010
11. Baccino R, Moret F (2000) Numerical modeling of powder metallurgy processes. Mater Des 21(4):359–364. doi:10.1016/S0261-3069(99)00094-1
12. Ratti M, Leuvrey D, Mathon MH, De Carlan Y (2009) Influence of titanium on nano-cluster (Y, Ti, O) stability in ODS ferritic materials. J Nucl Mater 386–388:540–543
13. Sornin D, Grosdidier T, Malaplate J, Tiba I, Bonnaillie P, Allain-Bonasso N, Nunes D (2013) Microstructural study of an ODS stainless steel obtained by hot uni-axial pressing. J Nucl Mater 439:19–24
14. Fields DS, Backofen WA (1979) Determination of strain hardening characteristics by TorsionTesting. Proc ASTM 57:583–591
15. Sung-Il K, Yeon-Chul Y (2002) Continuous dynamic recrystalliza-tion of AISI 430 ferritic stainless steel. Met Mater Int 8(1):7–13
16. Praud M (2012) Plasticité d'alliages renforcés par nano-précipitation Université Toulouse 3 Paul Sabatier
17. Kim SI, Lee Y, Byon SM (2003) Study on constitutive relation of AISI 4140 steel subject to large strain at elevated temperatures. J Mater Process Technol 1-3:84–89. doi:10.1016/S0924-0136(03)00742-8
18. Kajberg J, Sundin KG (2013) Material characterisation using high-temperature Split Hopkinson pressure bar. J Mater Process Technol 213(4):522–531. doi:10.1016/j.jmatprotec.2012.11.008
19. Bao Y, Wierzbicki T (2005) On the cut-off value of negative triaxi-ality for fracture. Eng Fract Mech 72(7):1049–1069